Non-Uniform Motion Monitoring Using the Permanent Scatterers Technique

A. Ferretti, C. Prati, F. Rocca
Dipartimento di Elettronica e Informazione - Politecnico di Milano
Piazza L. da Vinci, 32 - 20133 Milano - Italy
fax: +39-2-23993585, e-mail: aferre@elet.polimi.it

Abstract

Stable natural reflectors (Permanent Scatterers) can be identified from long temporal series of interferometric SAR images even with baselines larger than the decorrelation one. We discuss the use of PS in urban areas, like Pomona (California) showing subsidence and absidence effects. An estimation of the Atmospheric Phase Screen (APS) superimposed on each image and the displacement field in the area of interest is carried out. New solutions are presented in order to cope with non-uniform motion of the targets.

1 Introduction

One of the main difficulties encountered in DInSAR applications is due to temporal and geometric decorrelation. The main goal of our research was the identification of single pixels (to be called Permanent Scatterers - PS) coherent over long time intervals and for wide look-angle variations [1]. This allows one to use all ERS acquisitions relative to an area of interest. In fact when the dimension of the PS is smaller than the resolution cell, the coherence is good (the speckle is the same) even for image pairs taken with baselines larger than the decorrelation one. Then, on those pixels, sub-meter DEM accuracy and millimetric terrain motion detection can be achieved, even if the coherence is low in the surrounding areas. Reliable elevation and deformation measurements can then be obtained on this subset of image pixels that can be used as a "natural" GPS network.

2 Method

The mathematical framework for this kind of estimation is rather simple. Let us suppose that $N+1$ ERS SAR images of the area of interest are available. Data are first coregistered on a unique master and a DEM of the area is estimated starting from low temporal baseline pairs [3]. Then, N differential interferograms between all SAR images and the master are computed. After DEM compensation, the residual phase of interferogram i is [1]:

$$\phi_i = \frac{4\pi}{\lambda} r_{Ti} + \alpha_i + n_i + \varepsilon_{topo\_i} \qquad (1)$$

where λ is the system wavelength, α_i the atmospheric phase contribution, n_i the decorrelation noise, ε_{topo_i} the phase contribution due to possible errors in the DEM (proportional to the normal baseline of each image B_{n_i}) and r_{Ti} is the possible target motion in the direction of the satellite line-of-sight (LOS).

The first term in Eq. (1) can then be written as follows:

$$\frac{4\pi}{\lambda} r_{Ti} = \frac{4\pi}{\lambda} \cdot v_r \cdot T_i + \mu_{NLi} = C_{vi} \cdot v + \mu_{NLi} \qquad (2)$$

where v is the unknown component of the mean target velocity in the direction of LOS, μ_{NL} is the phase term due to a possible non-linear target motion and T_i is the temporal baseline between the master acquisition and the generic i-th slave image.

Since we have N differential interferograms of the same area with different temporal and geometric baselines, we finally write, for each pixel, a linear system of N equations and 2 unknowns (ε_z, v_r):

$$\phi_i = C_{zi} \cdot \varepsilon_z + C_{vi} \cdot v \qquad i = 1 \cdots N \qquad (3)$$

where ε_z is the DEM error and C_{zi} is proportional to B_{n_i}.

The problem would be linear if we knew the unwrapped phase values. Anyway, using a simple periodogram (albeit with an irregular sampling of the two dimensions: baselines and time) we can estimate both the residual elevation and the mean LOS velocity, provided that the signal-to-noise ratio is high enough.

Actually the Linear Phase Residues (LPR) w_i (i.e. phase data after linear detrending in temporal and spatial baseline) are the sum of three contributions: atmospheric components (Atmospheric Phase Screen - APS) of the master and the slave acquisitions,

noise, and non linear motion:

$$w_i = \phi_i - C_{zi} \cdot \varepsilon_z - C_{vi} \cdot v_r = \mu_{NLi} + \alpha_i + n_i \quad (4)$$

Since μ_{NL} , α and n are independent random variates, the residual phase variance σ_w^2 is the sum of three contributions: $\sigma_{\mu_{NL}}^2$, σ_{α}^2, and σ_n^2. As a matter of fact, a proper estimation of target motion and elevation is possible only if σ_w^2 is low. To this end, the analysis is carried out in two steps. First a subset of image pixels is selected using the coherence maps of the area of interest: only locations of highly coherent targets are retained (low σ_n^2). If now we consider a couple of targets not too far apart (distance less than, say, 1 km), it is usually possible to estimate Δv (relative mean velocity) and $\Delta\varepsilon_z$ (relative elevation error) with a high degree of accuracy. In fact, low distance implies low variance of the atmospheric component: for points less than 1 km apart, values of $\sigma_{\alpha.}^2$ less than 0.1 rad^2 are common [8]. Moreover, the motion of neighboring pixels is usually correlated. If this hypothesis is verified, $\sigma_{\mu.}^2$ should be low as well. Estimation of (v, ε_z) is then obtained integrating the values of (Δv, $\Delta\varepsilon_z$) previously estimated from couples of neighbor pixels [2]. Following this kind of approach, *we can actually unwrap the differential interferograms*. In fact, if condition $|w_i| < \pi$ is satisfied, we can easily recover the unwrapped phase differences $\Delta\phi_i$ between couples of neighbor pixels and then integrate them all over the sparse grid of PS candidates.

We can summarize the results as follows. Phase unwrapping of differential interferograms characterized by high geometrical and temporal baseline is possible only on a sparse grid of targets, previously selected as PS Candidates (PSC), and using a multi-image approach. The mathematical framework is easier if the constant velocity model can be applied. Anyway, this hypothesis is not a real constraint and the technique can cope with non-uniform target motion, provided that the PS density and coherence is high enough (low σ_w^2). Phase differences are unwrapped taking advantage of the estimated values of relative velocity Δv and relative elevation $\Delta\varepsilon_z$ of each scatterers pair. Phase data are then integrated using one of the techniques used for unwrapping regularly sampled data.

3 Space-Time Estimation

Once phase data are unwrapped, it is possible to estimate the signal of interest $s(\mathbf{x}, t)$ (e.g. $s = \alpha(\mathbf{x}, t)$ or $s = \mu(\mathbf{x}, t)$) using an optimum filter $\mathbf{f}$, properly weighting the data vector $\boldsymbol{\phi}$. In general, we may be interested in estimates at unmeasured points and instants too (interpolation and/or prediction). As well known, optimum weights f_i are the solution of the following system of equations [4][5]:

$$\mathbf{R}_{\phi\phi} \cdot \mathbf{f}(\mathbf{x}, t) = \mathbf{r}_{\phi\mathbf{s}}(\mathbf{x}, t) \quad (5)$$

where $\mathbf{R}_{\phi\phi} = E\left[\boldsymbol{\phi} \cdot \boldsymbol{\phi}^T\right]$ is the data correlation matrix and $\mathbf{r}_{\phi\mathbf{s}} = E\left[\boldsymbol{\phi} \cdot s(\mathbf{x}, t)\right]$ is the crosscorrelation vector between the data and the signal under estimation. It should be noted that the optimum filter $\mathbf{f}$ is space and time variant. In fact, since we deal with a sparse spatiotemporal distribution of samples, $\mathbf{r}$ is a function of $(\mathbf{x}, t)$. On the contrary $\mathbf{R}_{\phi\phi}$ is fixed, once the spatiotemporal data distribution is known.

The key point for optimum filtering is the estimation of the correlation values. While expression of the correlation matrix of the atmospheric component can be obtained from Kolmogorov theory [8], a statistical description of the local displacement field can be a very difficult task to achieve.

Basically, this choice should reflect our knowledge about the physical phenomenon we are dealing with (an example of mathematical modeling of a subsiding area is given in [7]). If a model is available, parameters and expression of the correlation matrix assume a specific physical meaning (see [6] and references therein). In Appendix A, the expression of $r\mu$ suited for a diffusion process is obtained starting from the Partial Differential Equation (PDE) describing this kind of phenomena. In general, the lack of a physical model does not allow an accurate estimation of the correlations and so the optimum filter can not be implemented.

Moreover, the computational burden of this estimation technique is huge due to the very large number of data involved. Inversion of matrix $\mathbf{R}_{\phi\phi}$ may be impractical even considering a moving neighborhood around the point under estimation.

If no a priori information is available about the displacement field of the area of interest, a possible approach that can be adopted is the whitening of the time series of the LPR samples $w(\mathbf{x}, t_i)$. Once the residual phases of the PSC have been obtained (data detrended for the estimated DEM errors and the mean velocity field), we can start looking at their temporal evolution, to check for subsidence leakage. The time smoothed component of $w(\mathbf{x}, t_i)$ should be considered as an estimation of the non-uniform motion contribution $\mu_{NL}(\mathbf{x}, t_i)$. APS estimation is then carried out *spatially smoothing the time high-pass filtered LPR data*:

$$\widehat{\alpha}(\mathbf{x}, t_i) = \left[\left[w(\mathbf{x}, t)\right]_{HP\_Time}\right]_{LP\_Space} \quad (6)$$

with obvious symbol meaning. To make it simple, we can carry out for each pixel a *temporal* smoothing using a triangular filter and remove the low pass component. Phase residuals are then *spatially* filtered using a moving average on a 2×2 km window.

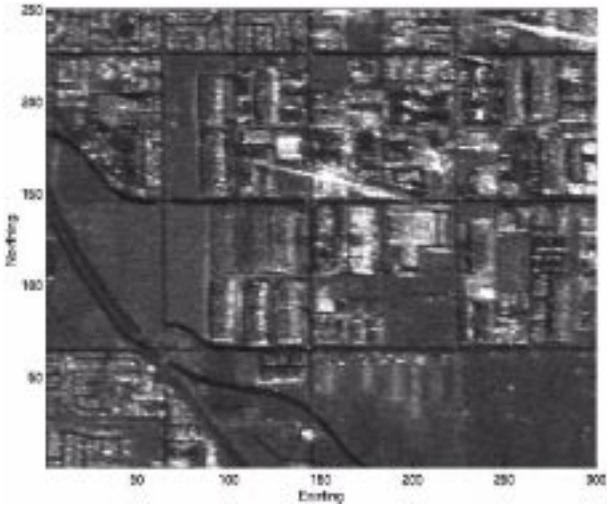

Figure 1: Geocoded multi-image reflectivity map of the test site (close up of Los Serranos area). The high radiometric quality is due to the incoherent data average.

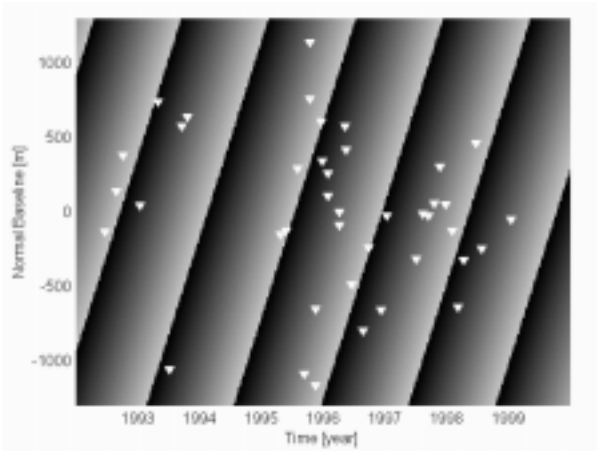

Figure 2: Space-Time distribution of the available data. The bidimemensional sinusoid represent the phase contribution for a LOS velocity of 2 cm/yr and a DEM error of 5 m (see text).

As described in [1], after estimation and removal of all the APS superimposed on the data, we can finally estimate the motion of each pixel in the image and identify more PS's. In fact the PSC set is just a rough estimation of the PS set since isolated coherent targets are not detected due to the space average used for coherence estimation.

4 Results

An interesting case of subsidence, already studied using differential interferometry and other techniques, is found in Pomona [9]. 41 ERS images were available (Track: 170. Frame: 2925). All were resampled on the same master acquisition (ERS2 - April 6th, 1996) and 40 interferograms were obtained. In Fig. 1 the incoherent average of all the data (close up of Los Serranos area) is reported: due to the high number of looks, the radiometric quality of this image is comparable to that of an optical one. Using 4 Tandem pairs, we also determined a reference DEM (about 10 m accuracy, also limited by building effects) of the area of interest using the wavelet approach [3], and the correspondent phase was removed from each single image.

After the initial selection of the PS set (about 3 PS/km^2 were identified), phase increments between each PS and all the others less than 1 km apart were estimated using the periodogram technique. To better illustrate this kind of approach, in Fig. 2 we show the temporal distribution of the takes together with their normal baselines, referred to the master image. The range of normal baselines is about +/- 1100 m, while the maximum temporal baseline is more than 6 years. If a PS had a LOS velocity of, say, 2 cm/yr and a residual elevation difference of 5 m with respect to a neighboring scatterer, considered as a reference, its phase variations as a function of time and baseline would be a 2D sinusoid, also represented in the Fig. 2. If now we accept, temporarily, the hypothesis of constant LOS velocity of each pixel, then using a periodogram we can estimate both the residual elevation and the LOS velocity difference of the pixels. As already mentioned, this operation was carried out for all PS pairs less than 1 km apart, thus removing the effects of the residual elevation with respect to the average DEM and of the LOS velocity and estimating the unwrapped phase values [2].

After estimation of both elevation and mean velocity of the targets, time series analysis of the phase residues in correspondence of each PS was carried out. The target is to identify possible non-linear motion contributions. As discussed previously, for each PS we carried out a temporal smoothing using a triangular filter (300 days long) and we removed the low pass component. Phase residuals were then spatially filtered using a moving average on a 2×2 km window. APS's were then interpolated on the original regular grid and removed from each datum. It should be noted that each APS is actually the difference of the atmospheric component of the slave image and the APS of the master acquisition. Averaging the 40 APS's it was possible to get an estimation of the master contribution and then of each single contribution. An example of estimated APS is reported in Fig. 3.

After APS removal it is possible to estimate not only the mean velocity field of the area but a dis-

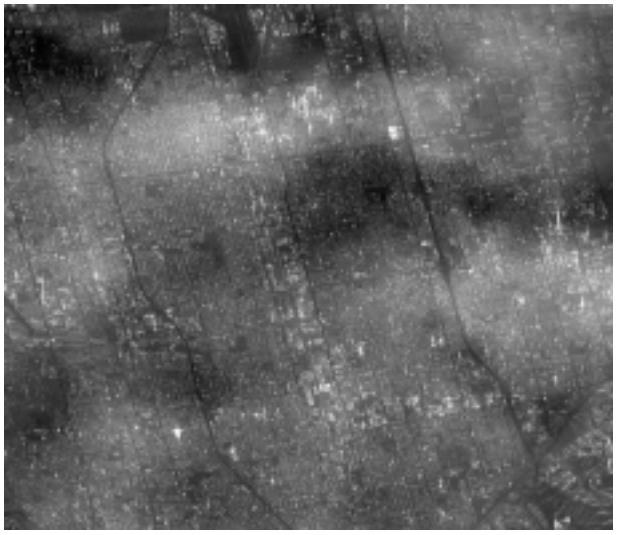

Figure 3: Example of APS estimated for April 6^{th}, 1996. The APS has been superimposed on the multi-image reflectivity map of the area. APS standard deviation is 0.86 *rad*.

placement field as a function of time, possibly interpolating the displacement maps on a regular temporal grid. Here we report a sequence of 4 spatial maps corresponding to 4 equally spaced time instants (Fig. 4, 5, 6 and 7). The non-linear motion behavior reflects into the change of shape of the contour lines. A perspective view of the displacement field of Fig. is also reported in Fig. 8. Maximum positive and negative displacements are +6 and -20 cm, respectively. Of course, computer animation procedures can provide an improved visualization of the phenomenon under study. Two animations relative to the estimated displacement field in Pomona since June 1992 will be soon available on our web site [10].

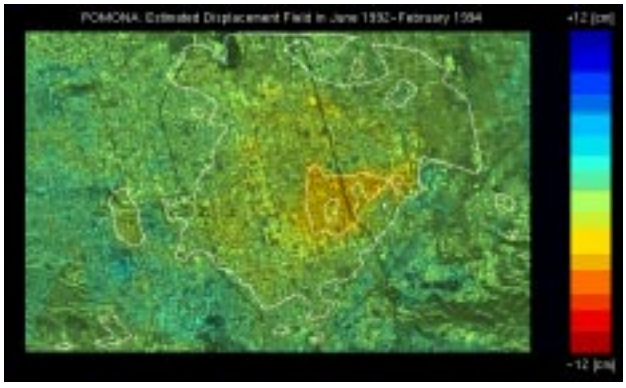

Figure 4: Pomona: estimated displacement field in *cm* relative to the time interval June 1992 - February 1994. Contour lines step: 2.5 *cm*.

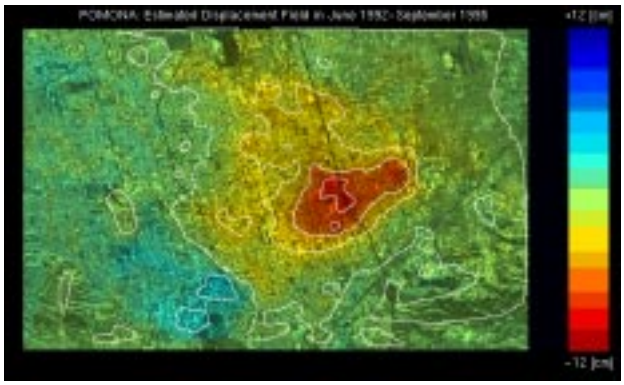

Figure 5: Pomona: estimated displacement field in *cm* relative to the time interval June 1992 - September 1995.

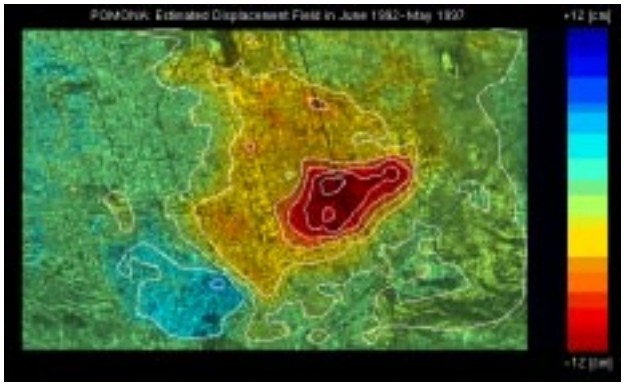

Figure 6: Pomona: estimated displacement field in *cm* relative to the time interval June 1992 - May 1997.

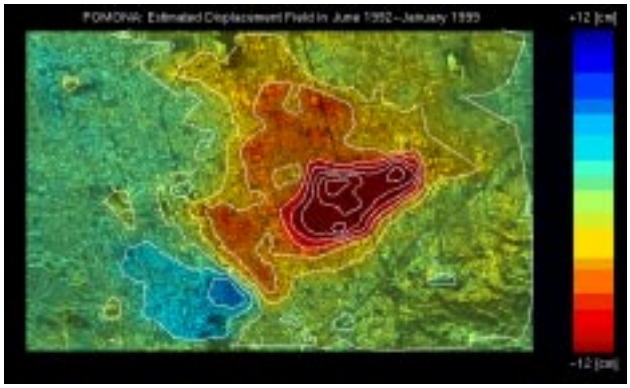

Figure 7: Pomona: estimated displacement field in *cm* relative to the time interval June 1992 - January 1999. Color scale has been satured for visualization purposes (+/- 12 cm).

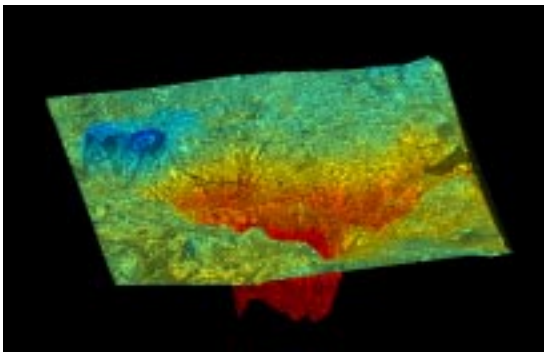

Figure 8: Perspective view of the displacement field relative to June 1992 - January 1999. Minimum negative value: -20 *cm*. Maximum positive displacement: +6 *cm*.

5 Conclusions

We have shown that in urban areas Permanent Scatterers exist that allow to generate interferograms on a sparse grid, even if the time lapse between the takes is many years long. The spatial dimensions of the scatterers can be selected to be small with respect to range resolution so that baselines longer than the critical one can be used. The density of those PS's, small enough to have sufficient phase stability with respect to the baseline, was seen to be sufficient (at least in urban areas) to be able to estimate the atmospheric disturbance (the APS) with a sufficient spatial resolution. Then, the estimated APS can be removed from the interferometric phase, improving the DEM estimates and improving the estimate of the pixel motion.

The long time lapse observations made available by this technique allow to estimate long term pixel motion with an accuracy that was previously attainable using optical techniques only. Sure enough, the density of the PS's may prove to be too low in vegetated areas, so that artificial PS's, namely corner reflectors, will have to be added in some locations. However, first tests indicate that rather small CR's, say with 1500 m^2 cross section, should suffice.

Several questions remain to be studied like: i) the distribution of PS's in different types of terrain, ii) the possibility of reducing the threshold coherence level to extend their number, iii) the physical nature of the PS's in towns and on rocky terrain, etc. iv) the quality of the APS estimates and their statistics.

6 Appendix A

In this section, we shall approximately model the dynamics of the subsidence mechanism with a diffusion process, in order to be able to derive the optimum filter. A diffusion process is governed by the following partial differential equation:

$$\frac{\partial^2 S}{\partial x^2} + \frac{\partial^2 S}{\partial y^2} = c\frac{\partial S}{\partial t}$$

in our case, we take S as the surface of the terrain and c as a diffusion coefficient. In the time wavenumber domain we have that the pulse response of the system is (V_0, volume of the infilled or of the extracted fluid, constant with time):

$$S(u,v,t) = V_0 \exp\left[-t\left(u^2+v^2\right)/c\right]$$

In the time space domain we have:

$$S(x,y,t) = \frac{c}{4\pi t} V_0 \exp\left[-c\left(x^2+y^2\right)/4t\right]$$

and finally in the frequency wavenumber domain we have

$$S(u,v,\omega) = \frac{V_0 c}{k^2 + j\omega c}$$

The power spectrum is: :

$$\begin{aligned} P_s &= \frac{|S|^2}{L_{tot}^2 T_{tot}} = \sigma^2 \frac{c^2}{k^4+\omega^2 c^2} \\ k^2 &= u^2 + v^2 \\ \sigma^2 &= \frac{\sum V_i^2}{L_{tot}^2 T_{tot}}. \end{aligned}$$

Notice that:

$$\sigma^2 \int_{\pi/L_{tot}}^{\pi/\Delta} \int_{-\infty}^{\infty} \frac{2\pi c^2 k}{k^4+\omega^2 c^2} \frac{d\omega}{2\pi} \frac{dk}{2\pi} = \frac{\sigma^2 c}{2} \int_{\pi/L_{tot}}^{\pi/\Delta} \frac{dk}{k} = \frac{\sigma^2 c}{2} \ln\left(\frac{L_{tot}}{\Delta}\right)$$

is the ms value of the non aliased subsidence. The atmospheric contribution has a power spectrum P_A that decreases with the wavwnumber k as $k^{-8/3}$; its contribution is independent from one take to the next.

$$P_A = \frac{Q_1}{k^{8/3}}$$

The optimum temporal filter will therefore be all pass for relatively high wavenumbers and low pass for low wavenumbers (where the atmospheric effect is most active). Indicating the measurements with $M(k,\omega)$, the Wiener estimate of the subsidence $\widehat{S}$ is:

$$\widehat{S} = \frac{P_s}{P_s + P_A} M = \frac{k^{8/3}}{k^{8/3} + Q(k^4+\omega^2 c^2)} M$$

where Q is a coefficient dependent on the Atmospheric Phase Screen and we took $c \simeq 4 \times 10^{-4} (m^2/month)$.

7 Acknowledgments

We'd like to thank Dr. G. Rigamonti and Dr. R. Locatelli for their support in data processing and Dr N. Bienati for helpful discussions.

References

[1] A. Ferretti, C. Prati and F. Rocca, "Permanent Scatterers in SAR Interferometry", submitted for publication to *IEEE Trans. Geosci. Remote Sensing*, June 1999.

[2] A. Ferretti, C. Prati and F. Rocca, "Non-linear Subsidence Rate Estimation Using Permanent Scatterers in Differential SAR Interferometry ", submitted for publication to *IEEE Trans. Geosci. Remote Sensing*, September 1999.

[3] A. Ferretti, C. Prati and F. Rocca, "Multibaseline InSAR DEM Reconstruction: the Wavelet Approach", *IEEE Trans. Geosci. Remote Sensing*, vol. 37, no. 2, pp. 705-715, Mar. 1999.

[4] S. Haykin, *Adaptive Filter Theory -2nd Edition,* Prentice Hall, 1991.

[5] H. Wackernagel, *Multivariate Geostatistics - 2nd Edition,* Springer-Verlag, 1998.

[6] G. Christakos and P. Bogaert, "Spatiotemporal Analysis of Spring Water Ion Processes Derived from Measurements at the Dyle Basin in Belgium," *IEEE Trans. Geosci. Remote Sensing*, vol. 34, no. 3, pp. 626-642, May 1996.

[7] G. Gambolati, G. Ricceri, W. Bertoni, G. Brighenti and E. Vuillermin, "Mathematical Simulation of the Subsidence of Ravenna," *Water Resour. Res.*, vol. 27, no. 11, pp. 2899-2918, 1991.

[8] S. Williams, Y. Bock and P. Pang, "Integrated satellite interferometry: Tropospheric noise, GPS estimates and implications for interferometric synthetic aperture radar products," *J. Geophys. Res.*, 103, B11, pp. 27.051-27.067, 1998.

[9] G. Peltzer, "Monitoring of Ground Subsidence," http://www.esrin.esa.it/esrin/eos/mon2.html

[10] POLIMI DSP Group Web Site: http://www-dsp.elet.polimi.it